Conjugate forced convection heat transfer from a continuous, moving flat sheet

Ming-I Char
Department of Applied Mathematics, National Chung Hsing University, Taichung, Taiwan, ROC

Cha'O-Kuang Chen
Department of Mechanical Engineering, National Cheng Kung University, Tainan, Taiwan, ROC

John W. Cleaver
Department of Mechanical Engineering, The University of Liverpool, Liverpool, UK

A cubic spline collocation numerical method has been used to determine the conjugate heat transfer occurring in the laminar boundary layer on a continuous, moving plate. Numerical results for the local heat flux and temperature distribution of both the moving plate and the fluid under the effects of the Peclet number (which determines the relative importance of the motion), the conjugate convection–conduction parameter (which depends on the properties of the fluid and the plate), and the Prandtl number are obtained by solving simultaneously the convective boundary-layer equation of the fluid and the energy equation of the plate. Results show that the Peclet number and the convection–conduction parameter have a significant influence on heat transfer characteristics. In addition, the heat transfer mechanism between the moving plate and the ambient fluid with air (Pr=0.7) as the fluid is substantially different from that with water (Pr=7.0) as the fluid.

Keywords: conjugate; forced convection; cubic spline collocation method

Introduction

Boundary-layer behavior on a moving continuous solid surface is an important type of flow that occurs in a number of engineering processes. A polymer sheet or filament extruded continuously from a die, or a long thread traveling between a feed roll and a wind-up roll, are examples of continuous, moving surfaces.

Flow in the boundary layer on a continuous solid surface with constant speed was studied by Sakiadis.[1] Due to entrainment of ambient fluid, this situation represents a different class of the boundary-layer problem, which has a solution substantially different from that of boundary-layer flow over a semi-infinite flat plate. Erickson, Fan, and Fox[2] extended this problem to the case with suction or blowing at the moving surface. However, polyester is a flexible material, so the filament surface may stretch during ejection, causing the surface velocity to vary. Crane[3] considered the moving strip whose velocity is proportional to the distance from the slit. This type of flow usually occurs in the drawing of plastic films and artificial fibers. The heat and mass transfer on a stretching sheet with suction or blowing was investigated by Gupta and Gupta.[4] They dealt with the isothermal moving plate and obtained temperature and concentration distributions. Dutta, Roy, and Gupta[5] analyzed the temperature distribution in the flow over a stretching sheet with uniform heat flux. They showed that the temperature at a point decreases with increase in Prandtl number.

More recently, Grubka and Bobba[6] considered the heat transfer occurring on the linear impermeable stretching surface with a power-law surface temperature. Heat transfer in flow past a continuously moving porous flat plate with constant heat flux was studied and similarity solutions were presented by Murty and Sarma.[7] The effects of both the power-law surface temperature and the power-law surface heat flux variation on the heat transfer characteristics of a continuous, linearly stretching sheet subject to suction or blowing was analyzed by Chen and Char.[8] They also reported several closed-form analytical solutions for special conditions.

In References 1–8, either the temperature distribution or the heat flux of the sheet was prespecified. However, because the temperature distribution of the sheet is not known *a priori*, solving the conductive–convective heat transfer as a coupled problem is necessary. This solution involves analysis of the temperature field on the fluid side and the temperature field in the sheet. In this study, we used a cubic spline collocation numerical method[9–12] to solve conjugate heat transfer at the fluid–solid interface. Numerical results showing the local heat flux and the temperature distribution of both the moving plate and the fluid as a function of the Prandtl number, the convection–conduction parameter, and the Peclet number is presented.

Analysis

Consider a sheet that issues from a slot continuously and moves through the environment of a cooling fluid, as shown in Figure 1. The adopted frame of axes is stationary, with the origin located at the surface of the sheet ($y=0$) and of the slot ($x=0$). We assumed that the boundary-layer approximations are still applicable and neglected viscous dissipation in the energy equation.

For steady, two-dimensional (2-D) incompressible Newtonian

Address reprint requests to Dr. Cleaver at the Department of Mechanical Engineering, Thermofluids Division, The University of Liverpool, P.O. Box 147, Liverpool L69 3BX, UK.

Received 11 July 1988; accepted 23 February 1990

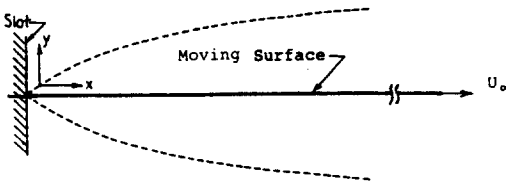

Figure 1 Boundary layer on a moving plate

flow on a continuous flat surface moving with a constant velocity U_o in a fluid medium at rest, the boundary-layer equation of motion is

$$u\frac{\partial u}{\partial x}+v\frac{\partial u}{\partial y}=\nu\frac{\partial^2 u}{\partial y^2} \tag{1}$$

the continuity equation is

$$\frac{\partial u}{\partial x}+\frac{\partial v}{\partial y}=0 \tag{2}$$

and the energy equation is

$$u\frac{\partial T}{\partial x}+v\frac{\partial T}{\partial y}=\alpha_f\frac{\partial^2 T}{\partial y^2} \tag{3}$$

The energy equation for the extruded sheet is based on the assumption that the thickness of the sheet, b, is small and the temperature is uniform across the cross section. Using the heat balance on the sheet, we obtain

$$\frac{2K_f}{bK_s}\frac{\partial T}{\partial y}\bigg|_{y=0}=-\frac{d^2T_s}{dx^2}+\frac{U_o}{\alpha_s}\frac{dT_s}{d_x} \tag{4}$$

where the subscript s refers to the sheet and f denotes the ambient fluid. We can generalize these equations by making them dimensionless:

$$X^*=\frac{x}{L}\qquad Y^*=\frac{y\mathrm{Re}^{1/2}}{L}\qquad \mathrm{Re}=\frac{U_oL}{\nu}\qquad U^*=\frac{u}{U_o}$$

$$V^*=\frac{v\mathrm{Re}^{1/2}}{U_o}\qquad \theta=\frac{(T-T_\infty)}{(T_o-T_\infty)}$$

The dimensionless equations are

- For the fluid:

$$U^*\frac{\partial U^*}{\partial X^*}+V^*\frac{\partial U^*}{\partial Y^*}=\frac{\partial^2 U^*}{\partial Y^{*2}} \tag{5}$$

$$\frac{\partial U^*}{\partial X^*}+\frac{\partial V^*}{\partial Y^*}=0 \tag{6}$$

$$U^*\frac{\partial \theta}{\partial X^*}+V^*\frac{\partial \theta}{\partial Y^*}=\frac{1}{\mathrm{Pr}}\frac{\partial^2\theta}{\partial Y^{*2}} \tag{7}$$

- Within the sheet:

$$2\mathrm{Re}^{1/2}\frac{K_f}{K_s}\frac{L}{b}\frac{\partial\theta}{\partial Y^*}\bigg|_{Y^*=0}=-\frac{d^2\theta_s}{dX^{*2}}+\mathrm{Pe}\frac{d\theta_s}{dX^*} \tag{8}$$

where $\mathrm{Pr}=\nu/\alpha_f$ and $\mathrm{Pe}=U_oL/\alpha_s$

The boundary conditions appropriate to Equations 5–8 are

$$\begin{aligned}
&U^*=1, \quad V^*=0 && \text{for } Y^*=0\\
&U^*=0, \quad \theta=0 && \text{as } Y^*\to\infty\\
&U^*=0, \quad V^*=0, \quad \theta=0, \quad \theta_s=1 && \text{for } X^*=0\\
&\frac{d\theta_s}{dX^*}=0 && \text{as } X^*\to\infty
\end{aligned} \tag{9}$$

The thermal conditions at the fluid–solid interface $y=0$ for continuity in temperature and heat flux give rise to

$$\theta=\theta_s \quad \text{and} \quad -K_f\frac{\partial\theta}{\partial y}=-K_s\frac{\partial\theta_s}{\partial y}$$

These conditions are obtained by the iterative procedure outlined in the next section.

From Equations 5–8, it is obvious that the leading physical parameters are Pr (the Prandtl number), Pe (the Peclet number), and $K_fL/\mathrm{Re}^{1/2}/K_sb$ (convection–conduction parameter, called CCP hereafter). We assigned to the Prandtl number the values of 0.7 and 7.0, which are typical for air and water; to the CCP, the values of 1.5, 2.0, 3.0, 5.0, and 8.0; and to the Peclet number, the values of 0.0, 0.001, 3.5, 6.0, and 10.0.

Numerical procedure

In the numerical solution of the governing Equations 5–7, we first used the false transient technique:[9] A fictitious transient

Notation

b	Thickness of the plate
C	Specific heat of the plate
CCP	Convection–conduction parameter, $\mathrm{Re}^{1/2}K_fL/K_sb$
K_f	Thermal conductivity of the fluid
K_s	Thermal conductivity of the plate
L	Length
Pe	Peclet number, U_oL/α_s
Pr	Prandtl number, ν/α_f
q	Local heat flux
Re	Reynolds number, U_oL/ν
T	Temperature
T_o	Temperature at point of emergence
U_o	Velocity of the plate
u, U^*	Dimensional and dimensionless velocities of the fluid in the x direction
v, V^*	Dimensional and dimensionless velocities of the fluid in the y direction
x, X^*	Dimensional and dimensionless coordinate distances along the moving plate
y, Y^*	Dimensional and dimensionless coordinate distances perpendicular to the plate surface

Greek symbols

α	Thermal diffusivity, $K/\rho C$
θ	Dimensionless temperature, $(T-T_\infty)/(T_o-T_\infty)$
ν	Kinematic viscosity of the fluid
ρ	Density

Superscript

*	Dimensionless quantity

Subscripts

∞	Ambient condition
s	Plate
f	Fluid

term is inserted on the left-hand side of Equations 5, 7, and 8. We then solved these nonlinear partial differential equations with a numerical integration technique by using the cubic spline. In general, the main advantages of using a cubic spline collocation are that:[10]

(1) The governing matrix system obtained is always tridiagonal, permitting the use of the Thomas algorithm in the inversion procedure.

(2) For a uniform mesh, the spline approximation is of fourth-order accuracy for the first derivative and of third-order accuracy for a nonuniform grid. The second derivative is of second-order accuracy for uniform as well as nonuniform grids.

(3) As the values of the first and second derivatives may be evaluated directly, boundary conditions containing derivatives may also be directly incorporated into the procedure.

Equations 5–8 using the false transient technique in discrete form, where the terms $\partial U^*/\partial X^*$, $\partial V^*/\partial Y^*$, and $\partial\theta/\partial X^*$ are represented by their finite-difference approximations, are

$$\frac{U_{i,j}^{*n+1}-U_{i,j}^{*n}}{\Delta\tau}+U_{i,j}^{*n}\frac{U_{i,j}^{*n}-U_{i-1,j}^{*n}}{\Delta X^*}+V_{i,j}^{*n}l_{U_{i,j}}^{n+1}=L_{U_{i,j}}^{n+1} \tag{10}$$

$$\frac{U_{i,j}^{*n+1}-U_{i-1,j}^{*n+1}}{\Delta X^*}+\frac{V_{i,j}^{*n+1}-V_{i,j-1}^{*n+1}}{\Delta Y^*}=0 \tag{11}$$

$$\frac{\theta_{i,j}^{n+1}-\theta_{i,j}^{n}}{\Delta\tau}+U_{i,j}^{*n+1}\frac{\theta_{i,j}^{n}-\theta_{i-1,j}^{n}}{\Delta X^*}+V_{i,j}^{*n+1}l_{\theta_{i,j}}^{n+1}=\frac{1}{\mathrm{Pr}}L_{\theta_{i,j}}^{n+1} \tag{12}$$

$$\frac{\theta_{s_i}^{n+1}-\theta_{s_i}^{n}}{\Delta\tau}=M_{\theta_{s_i}}^{n+1}-\mathrm{Pe}(m_{\theta_{s_i}}^{n+1})+2\mathrm{CCP}l_{\theta_{i,1}}^{n+1} \tag{13}$$

where

$$\Delta X^*X_i^*-X_{i-1}^* \qquad \Delta Y^*=Y_j^*-Y_{j-1}^*$$

$$l_{U^*}=\frac{\partial U^*}{\partial Y^*} \qquad L_{U^*}=\frac{\partial^2 U^*}{\partial Y^{*2}}$$

$$l_\theta=\frac{\partial\theta}{\partial Y^*} \qquad L_\theta=\frac{\partial^2\theta}{\partial Y^{*2}}$$

$$m_{\theta_s}=\frac{d\theta_s}{dX^*} \qquad M_{\theta_s}=\frac{d^2\theta_s}{dX^{*2}}$$

and $\Delta\tau=\tau^{n+1}-\tau^n$, representing the false time step. After some rearrangement, we can express these discrete equations in the form:

$$f_{i,j}^{n+1}=F_{i,j}+G_{i,j}l_{f_{i,j}}^{n+1}+S_{i,j}L_{f_{i,j}}^{n+1} \tag{14}$$

where f represents the function (U^*, θ). The quantities $F_{i,j}$, $G_{i,j}$, and $S_{i,j}$, are known coefficients, which are evaluated at previous time steps.

Equation 14, when combined with the cubic spline relations described in Reference 10, may be written in the tridiagonal form as

$$a_{i,j}\phi_{i,j-1}^{n+1}+b_{i,j}\phi_{i,j}^{n+1}+c_{i,j}\phi_{i,j+1}^{n+1}=d_{i,j} \tag{15}$$

where ϕ represents the function (U^*, θ, θ_s) and its first and second order derivatives. Equation 15 can be easily solved by the Thomas algorithm.

Because of the nonlinearities and the conjugate heat transfer between the moving sheet and the quiescent fluid, the energy equation for the fluid and heat conduction equation within the sheet have to be solved iteratively. The following is the numerical procedure used.

(1) Start by solving the momentum equation and obtaining velocity component U^*.

(2) Solve the continuity equation to get the velocity component V^*.

(3) Repeat steps 1 and 2 until the solution ceases to change significantly, i.e., until

$$\left|\frac{\phi_{ij}^{n}-\phi_{ij}^{n-1}}{\phi_{\max}^{n}}\right|<10^{-5} \tag{16}$$

where ϕ refers to U^* and V^* and n denotes the number of the false-time step.

(4) Estimate a sheet-temperature distribution $\theta_s(x)$.

(5) Solve the convective heat transfer equation for the fluid with the estimated sheet temperature as a wall boundary condition until convergence is achieved, i.e., until

$$\left|\frac{\phi_{ij}^{n}-\theta_{ij}^{n-1}}{\phi_{\max}^{n}}\right|<10^{-5} \tag{17}$$

(6) Calculate the heat flux $(\partial\theta/\partial Y^*)_0$ at every position X^*.

(7) Solve the heat conduction equation within the sheet with respect to these heat fluxes, which gives a new temperature distribution $\theta_s(x)$.

(8) Repeat steps 5–7 until the maximum relative change in the sheet temperature satisfies the criterion:

$$\left|\frac{\theta_s^{n}-\theta_s^{n-1}}{\theta_{s_{\max}}^{n}}\right|<10^{-5} \tag{18}$$

The conditions of continuity in heat flux and temperature at the fluid–solid interface are then satisfied and all relevant heat transfer characteristics can be calculated.

In this study, the computational region, $X^*>0$ and $Y^*>0$ is subdivided by means of a uniform grid. The extent of the grid in the Y^* direction is chosen so that the ambient conditions can be specified at a distance at least twice the estimated thickness of the boundary layer. The downstream condition in the X^* direction is specified at the extended length at which the temperature gradient becomes zero on every grid. The computations are performed with 61×31 grid points. The 31 grid points are utilized in the Y^* direction. Supplementary runs are performed with 51×26 grid points to investigate grid-size effects for the case of $\mathrm{Pr}=0.7$ and $\mathrm{Pe}=0.001$. The changes in the temperature gradient at $X^*=0$, $(-d\theta_s/dX^*)_0$, between the fine mesh (61×31) and the coarse mesh (51×26) are 0.30%, 0.31%, and 0.32% at CCP = 3.0, 5.0, and 10.0, respectively.

Results and discussion

The numerical procedure described was performed on a CDC cyber-172 computer. Downstream variation of surface temperature on a moving continuous flat plate for $\mathrm{Pr}=0.7$ and $\mathrm{Pe}=0.001$ at different CCP values is shown in Figure 2. The dimensionless temperature decreases monotonically from 1 at $X^*=0$ to zero with increasing X^*. By increasing CCP (with more insulation or greater convective cooling) the temperature of the plate falls. As the CCP increases, the distance X^* at which the temperature attains the ambient temperature decreases and the extent of the downstream rise becomes greater.

Distribution of the dimensionless local heat fluxes along the moving plate is illustrated in Figure 3. The dimensionless local heat fluxes in the Y^* direction at the plate surface $(Y^*=0)$ can be taken as

$$\frac{q(x)L}{K_f(T_o-T_\infty)\mathrm{Re}^{1/2}}=-\left(\frac{\partial\theta}{\partial Y^*}\right)_0 \tag{19}$$

With increasing X^*, the local heat flux profile at first decreases, reaches a minimum value, and then increases to a final zero value. Note in Figure 3 that, for positive local heat fluxes at

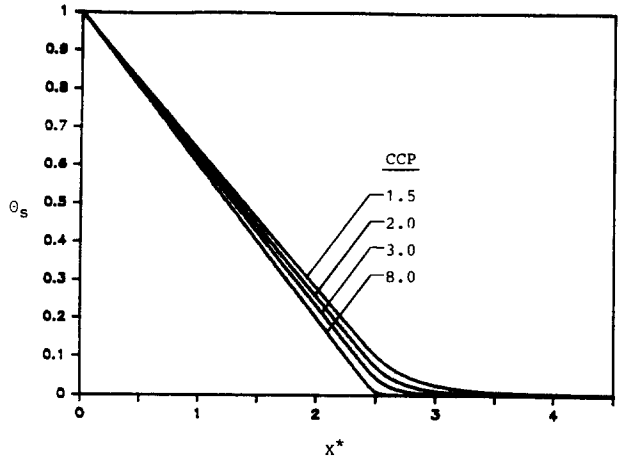

Figure 2 Downstream variation of surface temperature on a continuous, moving flat sheet at Pr=0.7 and Pe=0.001

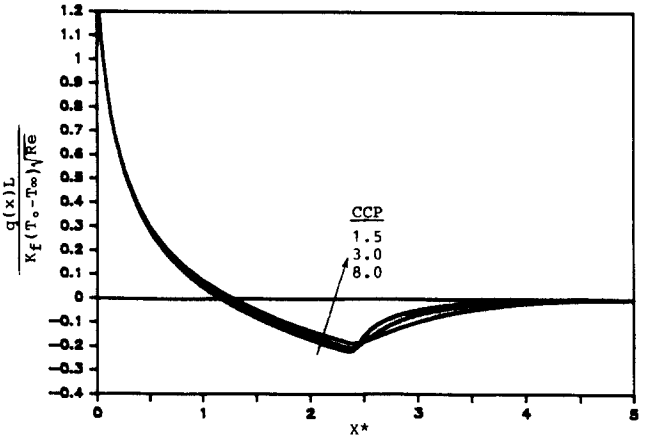

Figure 3 Downstream variation of the dimensionless local heat flux at Pr=0.7 and Pe=0.001

the upstream region, heat flows from the continuous surface to the ambient fluid. As X^* increases, the sign of the local heat flux changes and heat flows into the continuous surface from the ambient fluid.

This result occurs because the heated fluid accumulates in the boundary layer, giving rise to a boundary-layer temperature higher than the local plate temperature. Eventually—far downstream—the boundary-layer temperature and the plate temperature are in equilibrium. This condition is clearly shown in Figure 4.

Figure 4 indicates the fluid temperature distribution as a function of Y^* for the selected values of X^* at Pr=0.7, CCP=1.5, and Pe=0.001. When $X^*=0.8$, the wall temperature gradient is negative. A maximum temperature exists at the continuous surface, from which the fluid temperature decreases monotonically to the ambient temperature. Conversely, the wall temperature gradient in the Y^* direction becomes positive when $X^*=2.0$ and 2.8, which reflects the heat flow into the moving sheet from the ambient fluid. Hence the temperature profiles show that the maximum temperature occurs at a point within the boundary layer rather than on the plate.

Figure 5 shows the effect of the speed of the moving plate, as indicated by the Peclet number, on the temperature profiles at Pr=7.0 and CCP=5.0. As Pe increases, the magnitude of the temperature gradient at $X^*=0$, $(-d\theta_s/dX^*)_0$, decreases. This result indicates a decrease in the energy inflow into the plate due to conduction, although the total energy input (from convection and conduction) increased because of the increase in speed. As speed increases, we expect the temperature gradient to flatten somewhat and the temperature of the plate to increase. The reason is that, at larger values of Pe, for a given location along X^*, the plate is exposed for less time to the cooler environment. Therefore the material element gets less time for energy transfer from the surface. For the limiting case Pe=0, the problem is similar to forced convective heat transfer to a stationary plate.

Downstream variation of the dimensionless local heat flux for Pr=7.0 and CCP=5.0 at different values of the Peclet number is presented in Figure 6. For a given Pe value, the dimensionless local heat flux along the X^* direction decreases monotonically. The reasons are: (1) the local heat flux is positive, because heat flows from the plate surface to the ambient fluid; and (2) the surface temperature decreases, but the fluid temperature increases along the X^* direction. As Pe increases, the local heat flux is higher at a given location. The reason is that, for a given fluid and velocity U_o (i.e., Pr, K_f, and U_o unchanged), an increase in Pe must be accompanied by an increase in the thermal capacity $\rho_s C$ of the material as well, if CCP $[\mathrm{CCP}=K_f L\mathrm{Re}^{1/2}/(bK_s)]$ is to remain unchanged. An increase in thermal capacity of the material implies a higher surface temperature and then a greater loss of energy to the fluid.

Figure 7 displays the fluid temperature profiles along the Y^* direction for the selected values of X^* at Pr=7, CCP=5.0,

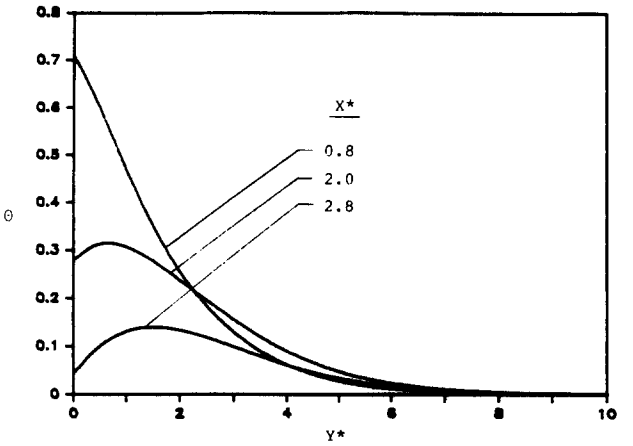

Figure 4 Temperature distribution along the Y^* direction within the fluid at Pr=0.7, CCP=1.5, and Pe=0.001

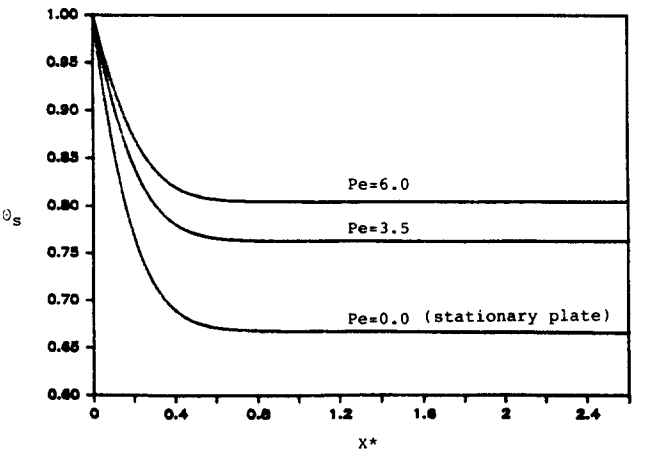

Figure 5 Downstream variation of surface temperature on a continuous, moving flat plate at Pr=7.0 and CCP=5.0

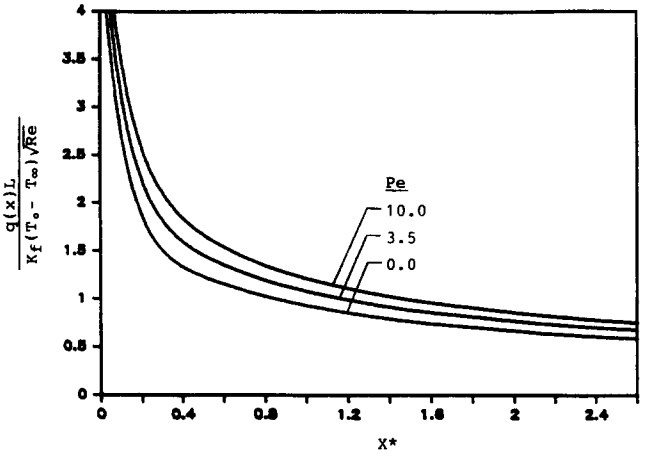

Figure 6 Downstream variation of the dimensionless local heat flux at Pr=7.0 and CCP=5.0

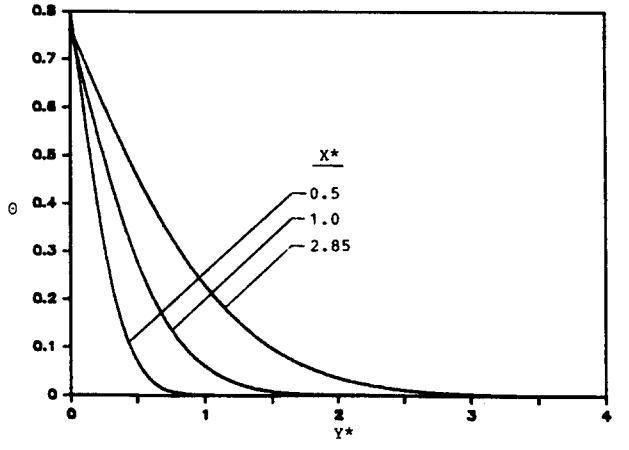

Figure 7 Temperature distribution along the Y^* direction within the fluid at Pr=7.0, CCP=5.0, and Pe=3.5

and Pe=3.5. The temperature at a given location, X^*, decays gradually with distance along the Y^* direction. In addition, the thermal boundary-layer thickness becomes thicker as X^* increases.

Conclusions

This research involved numerical investigation of the influence of the Prandtl number (Pr), the convection–conduction parameter ($CCP = Re^{1/2} K_f L / K_s b$), and the Peclet number (Pe) on heat transfer from a continuous, moving surface.

We showed that, for a given fluid at a constant Pe, a decrease in the thermal conductivity of the moving plate results in a decrease in the temperature in the axial direction. For a given fluid and for a fixed value of the CCP, an increase in the speed of the moving plate leads to a decrease in the energy inflow into the plate (due to conduction), an increase in the temperature in the axial direction, and an increase in the local heat flux. In addition, the mechanism of heat transfer between the moving plate and the ambient fluid with air (Pr=0.7) as the fluid is different from that with water (Pr=7) as the fluid.

References

1 Sakiadis, B. C. Boundary-layer behaviour on continuous solid surfaces: I. Boundary layer equations for two dimensional and axisymmetric flow. *AIChE J.*, 1961, **7**, 26

2 Erickson, L. E., Fan, L. T., and Fox, V. G. Heat and mass transfer on a moving continuous flat plate with suction or injection. *Ind. Eng. Chem. Fund.*, 1966, **5**, 19

3 Crane, L. J. and Angew, Z. Flow past a stretching plate. *Math. Phys.*, 1970, **21**, 645–647

4 Gupta, P. S. and Gupta, A. S. Heat and mass transfer on a stretching sheet with suction or blowing. *Can. J. Chem. Eng.*, 1977, **55**, 744

5 Dutta, B. K., Roy, P. and Gupta, A. S. Temperature field in flow over a stretching sheet with uniform heat flux. *Int. Comm. Heat Mass Transfer*, 1985, **12**, 89–94

6 Grubka, L. J. and Bobba, K. M. Heat transfer characteristics of continuous, stretching surface with variable temperature. *ASME Trans.*, 1985, **107**, 248–250

7 Vleggar, J. Laminar boundary layer behaviour on continuous accelerating surfaces. *Chem. Eng. Sci.*, 1977, **32**, 1517–1525

8 Chen, C. K. and Char, M. I. Heat transfer of a continuous stretching surface with suction or blowing. *J. Math. Anal. and Applic.*, 1988, **135**, 568–580

9 Rubin, S. G. and Graves, R. A. Viscous flow solution with a cubic spline approximation. *Computers and Fluids*, 1975, **3**, 1–36

10 Wang, P. and Kahawita, R. Numerical integration of partial differential equations using cubic splines. *Int. J. Computer Math.*, 1983, **13**, 271–286

11 Char, M. I. and Chen, C. K. Temperature field in non-Newtonian flow over a stretching plate with variable heat flux. *Int. J. Heat Mass Transfer*, 1988, **31**, 917–921

12 Rubin, G. S. and Khosla, P. K. Higher-order numerical solutions using cubic splines. *AIAA*, 1976, **14**, 851–858